BaBar note #194

Study of the iron segmentation optimization of the I.F.R. detector for μ / π discrimination.

Luca Lista
Salvatore Mele

Dipartimento di Scienze Fisiche,
Università degli Studi di Napoli "Federico II", Italy
and
I.N.F.N. Sezione di Napoli

3 november 1994

Abstract

We present a study of the iron segmentation optimization for the Instrumented Flux Return (I.F.R.) of BaBar. This study is based on a detector simulation performed with the `bbsim`[1] program using `GHEISHA` as simulation package for hadron interactions. We define discriminating variables to identify muons and reject pions. Different configurations have been studied, with both constant and graded segmentations. We found optimal configurations for graded thickness around 20 Fe planes with 21 detector layers. An efficient μ identification down to $p \sim 500$ MeV/c is obtained with a residual π detection efficiency of about 2%.

[1]developed mainly at LLNL by T.Wenaus and D.Wright

Contents

1 Introduction

One of the main purposes of the muon and neutral hadron detector for BABAR is to efficiently identify muons down to $p \sim 500$ MeV/c in order to allow B tagging with both direct $b \to \mu$ semileptonic decays and cascade $b \to c \to \mu$ decays. While the momentum spectrum of muons from direct decays is peaked at $p \sim 1.2$ GeV/c, the cascade decays have much lower momenta, as it can be seen from figure 1.

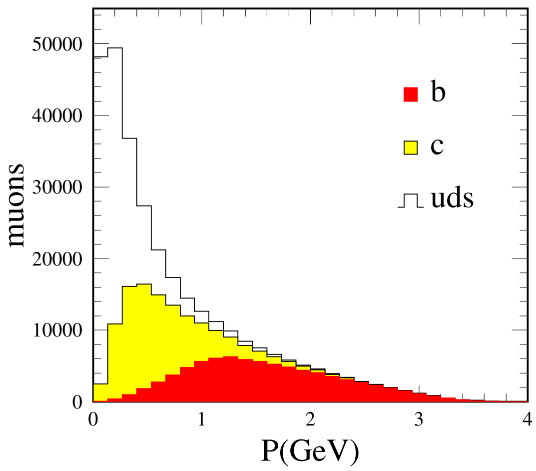

Figure 1: Momentum spectrum for muons in $\Upsilon(4S) \to \mathrm{B}^0\bar{\mathrm{B}}^0$ decays.

A study of kinematical variables shows that the two decays are very well separable giving a negligible amount of wrong-sign fraction [1]. The identification of cascade muons down to $p \sim 500$ MeV/c would increase the effective B tagging efficiency from 5% (as quoted in the L.O.I.) to about 9%.

In order to identify such low momentum muons, a thin iron segmentation is required. Thin segmentation is also the requirement for K_L^0 detection in order to have the best efficiency for the CP eigenstate decay $\mathrm{B}^0 \to \psi K_L^0$ [2].

2 Simulation

In order to study the highest possible number of segmentation configurations, we selected in the simulations program `bbsim` [3] an I.F.R. geometry consisting of 61 detector layers of 1.2 cm thickness alternated with 60 planes of iron of 1 cm thickness. Fe/detector thickness ratio is taken as the L.O.I. design with 24 Fe planes of 2.5 cm and 25 detector layers of 3 cm.

All the configurations with iron thickness multiple of 1 cm can be reproduced, with one run only, by switching off the undesired planes at analysis level. Throughout this work the barrel and the endcaps have the same segmentation.

We have simulated, using the `beget` generator [4], 40 000 $\mathrm{B}^0\bar{\mathrm{B}}^0$ events followed by the B^0 decaying into any of the possible decay channels and the $\bar{\mathrm{B}}^0$ becoming invisible to the detector. In this way we concentrate on the B^0 tagging assuming to have completely reconstructed the CP eigenstate decay products of the $\bar{B}^0$.

Since no pattern recognition has been used, we used GEANT information to associate each hit to the corresponding track. We do not expect a very high charged track multiplicity per event in the I.F.R., hence we assume that hit mis-assignment gives a negligible error.

Each position measurement is discretized within 5 cm two-dimensional pickup strips.

GHEISHA package for the simulation of hadron interaction has been used.

3 μ identification and π rejection

Several discriminating variables can be used for μ identification and π rejection [5]. These variables are based on the different interaction mechanisms of muons and pions in the Fe. We mainly distinguish five categories:

1. penetration in the Fe;
2. track continuity;
3. likelihood ratio of the number of hits in each plane;
4. tracking in the iron;
5. inner detector information;

3.1 Penetration in the Fe

Muons traversing the iron are only subject to energy loss until they stop and eventually decay, or escape the detector if they have enough energy. Pions can interact strongly with iron nuclei giving as result an hadron shower. A fraction of about 3.5% of pions decays into muons before reaching the coil. Muons from pion decays behave like muons produced at B decay vertex, but their momenta are lower than the parent hadron.

Figure 2 shows the distribution of the number of the last detector plane reached as a function of the momentum for μ and π. Muons stop in the I.F.R. for p below ~ 1.3 GeV/c, while for larger momenta they traverse all 60 cm of iron; pions have a higher probability to interact in the iron before escaping the detector.

A more appropriate variable is the penetration depth in the iron. The charged track measured in the Drift Chamber is fit with GEANE [6] package and extrapolated up to the I.F.R. . The number of interaction length traversed is computed and expressed in cm of Fe equivalent, using bbsim routines. In the I.F.R. the consecutive hits are connected with a poly-line, and the amount of Fe traversed is computed.

Figure 3 shows the total amount of material traversed as a function of p. Muon and pion distributions look very different. For muons, the depth in the iron increases with p up to $p \sim 1.3$ GeV/c where it reaches its (θ dependent) maximum (figure 4).

π rejection can be obtained in a straightforward way (figures 3 and 4). Cuts are optimized as a function of the iron configuration used.

In figure 4 the upper and lower depth cuts for $p > 1.5$ GeV/c are shown as solid lines; the effect of the gap in the CsI has been taken into account around $\cos\theta = 0.86$.

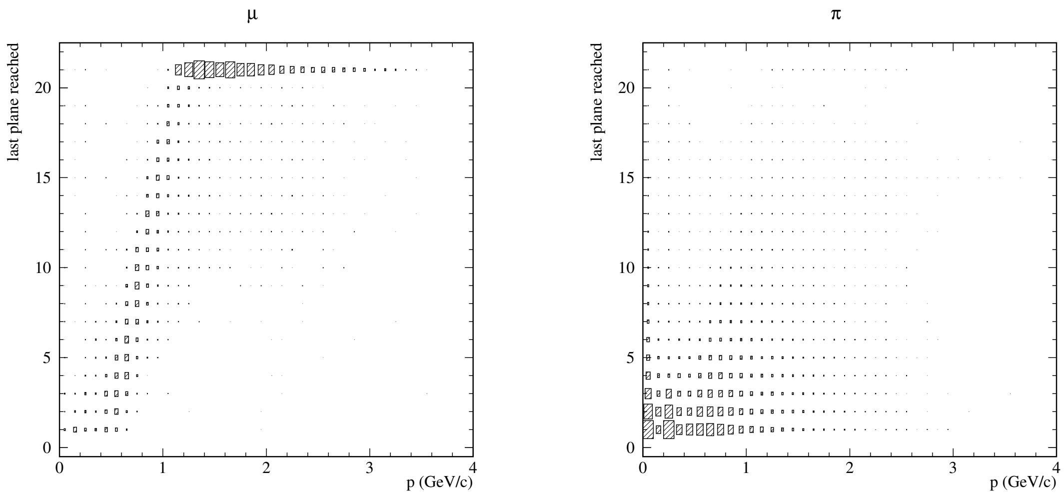

Figure 2: Distribution of the number of the last detector plane reached as a function of momentum for μ and π. The configuration used is 20×3 cm Fe planes.

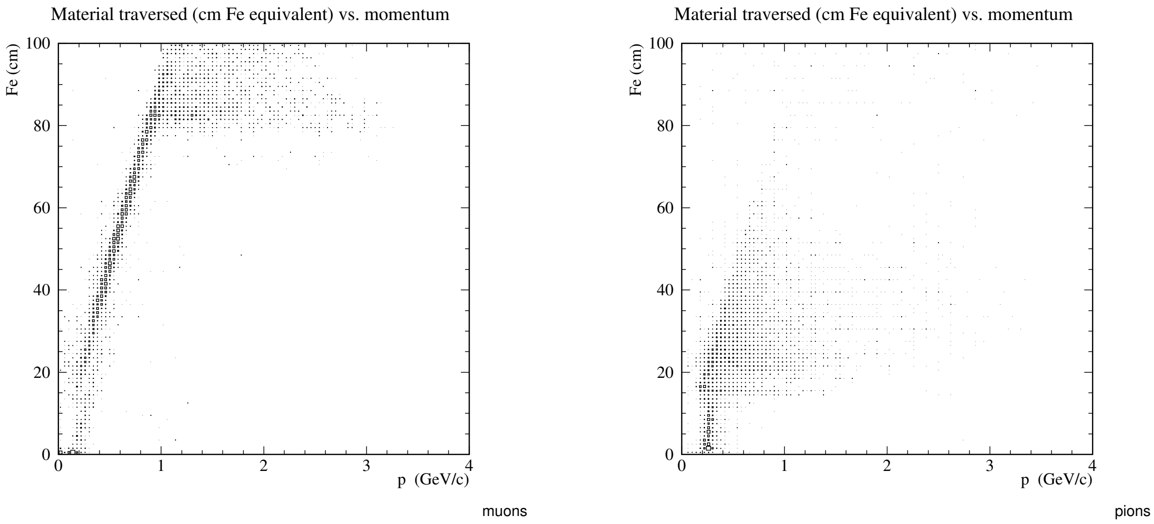

Figure 3: Depth in the iron (cm of Fe equivalent). The configuration used is 20×3 cm Fe planes.

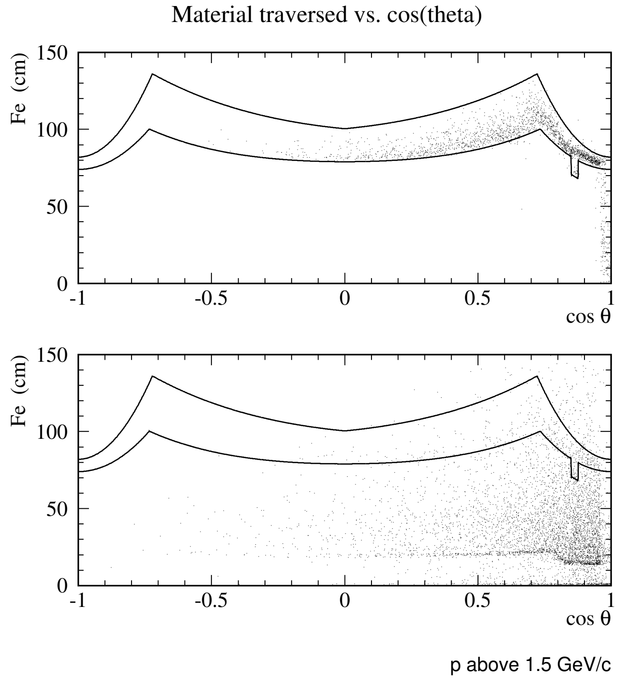

Figure 4: Depth in the iron for $p > 1.5$ GeV/c as function of $\cos\theta$.

3.2 Track continuity

Pion started hadron showers can turn completely neutral, so the pion track can be characterized by missed planes among planes hit.

In general, pion tracks have a number of hit planes smaller than the number of planes they span, while muon tracks hit roughly all the planes they traverse. A cut on the difference "*n. of planed spanned — n. of planes hit*" [7] gives a powerful pion rejection. A pictorial way to show the difference between muon and pion track patterns can be seen in figure 5, where the number of planes hit versus number of planes spanned is shown[1]. Figure 6 shows the maximum number, along the track, of consecutive missed planes; about 10% of pions have at least one missing plane along the track.

An inefficiency of the detector layers would, of course, worsen the power of μ/π discrimination these variables can give. This effect will be discussed later, in section 6.

[1]This plot is also known as "Calcaterra plot".

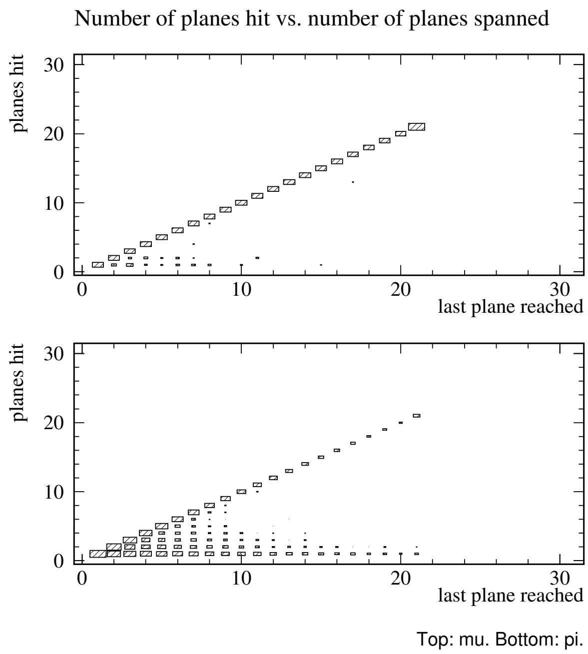

Figure 5: Number of planes hit *vs* number of planes spanned[1]. The configuration used is 20×3 cm Fe planes; 100% detector efficiency is assumed.

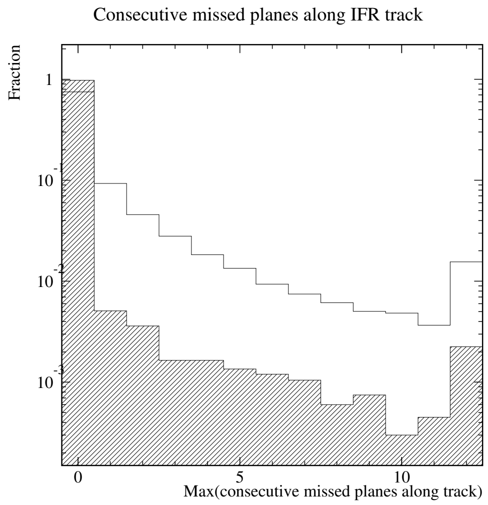

Figure 6: Maximum number of consecutive missed planes along the track. Empty: π; hatched: μ. Distributions are normalized to 1. The configuration used is 20×3 cm Fe planes; 100% RPC efficiency is assumed.

[1]The size of the squares is proportional to the log of the number of entries.

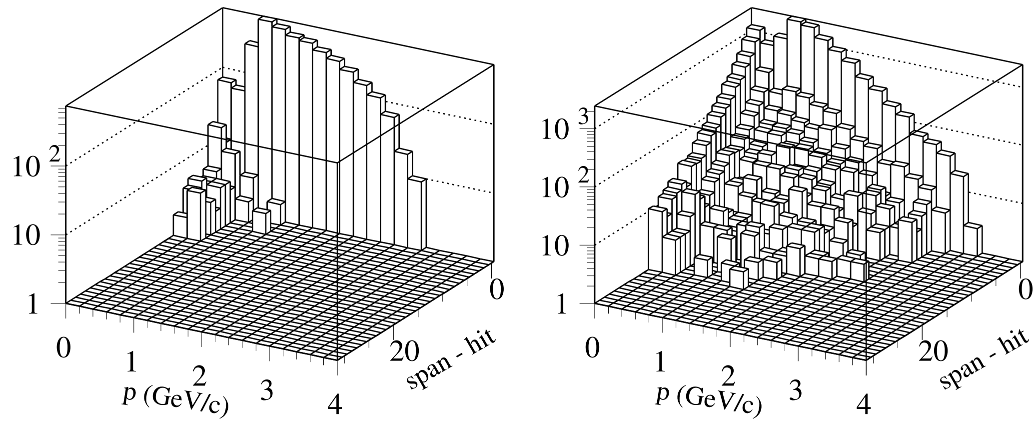

Figure 7: (Number of planes spanned - number of planes hit) *vs* p; left: muons, right: pions.

3.3 Likelihood ratio of the number of hits in each plane

A likelihood function can be built from the study of the number of hits in each plane for muons and pions. The momentum range has been split in four momentum bins, namely:

$$[0.5, 0.75], [0.75, 1.0], [1.0, 1.3] \text{ and } [1.3, 4.0] \text{ GeV/c}.$$

The first three bins have been chosen according to the observed different behavior of muons in the three ranges; the last one is the one in which μ are not stopped in the I.F.R.

Plane by plane, we determine from our Monte Carlo sample the probabilities $\mathcal{P}_i^{\mu}(n_i)$ and $\mathcal{P}_i^{\pi}(n_i)$ that a μ or a π gives n_i hits in the i-th plane; since more than 3 hits have been seldom observed, we saturate n_i at 3. If a plane is not reached by the particle, its corresponding n_i is set to -1 to distinguish this case from the one in which the plane is just missed ($n_i = 0$).

The probabilities distributions in the four bins for μ and π are plotted in figures 8 and 9. For a given track with $m_1 \dots m_N$ hits in the N planes, the likelihood to be a μ or a π given by:

$$\text{Prob}(\mu) = \prod_{j=1}^{N} \mathcal{P}_j^{\mu}(m_j) \qquad \text{and} \qquad \text{Prob}(\pi) = \prod_{j=1}^{N} \mathcal{P}_j^{\pi}(m_j).$$

A log-likelihood ratio function can be defined as:

$$\log_{10}(\text{Prob}(\pi)/\text{Prob}(\mu))$$

The value of this function can be seen in figure 10. The rejection power of this variable decreases if thicker segmentations are considered.

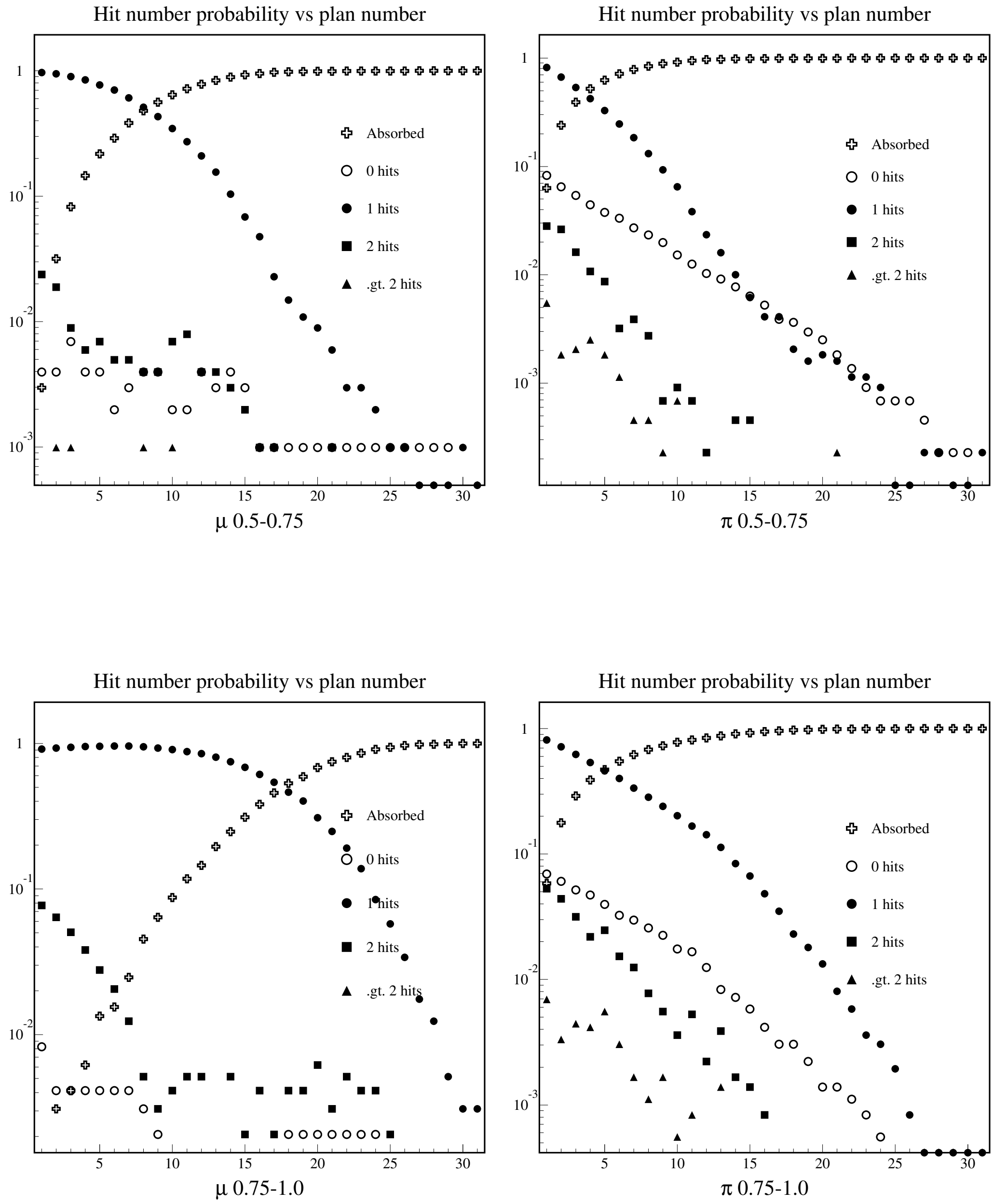

Figure 8: Probability distributions for the number of hits in each plane.

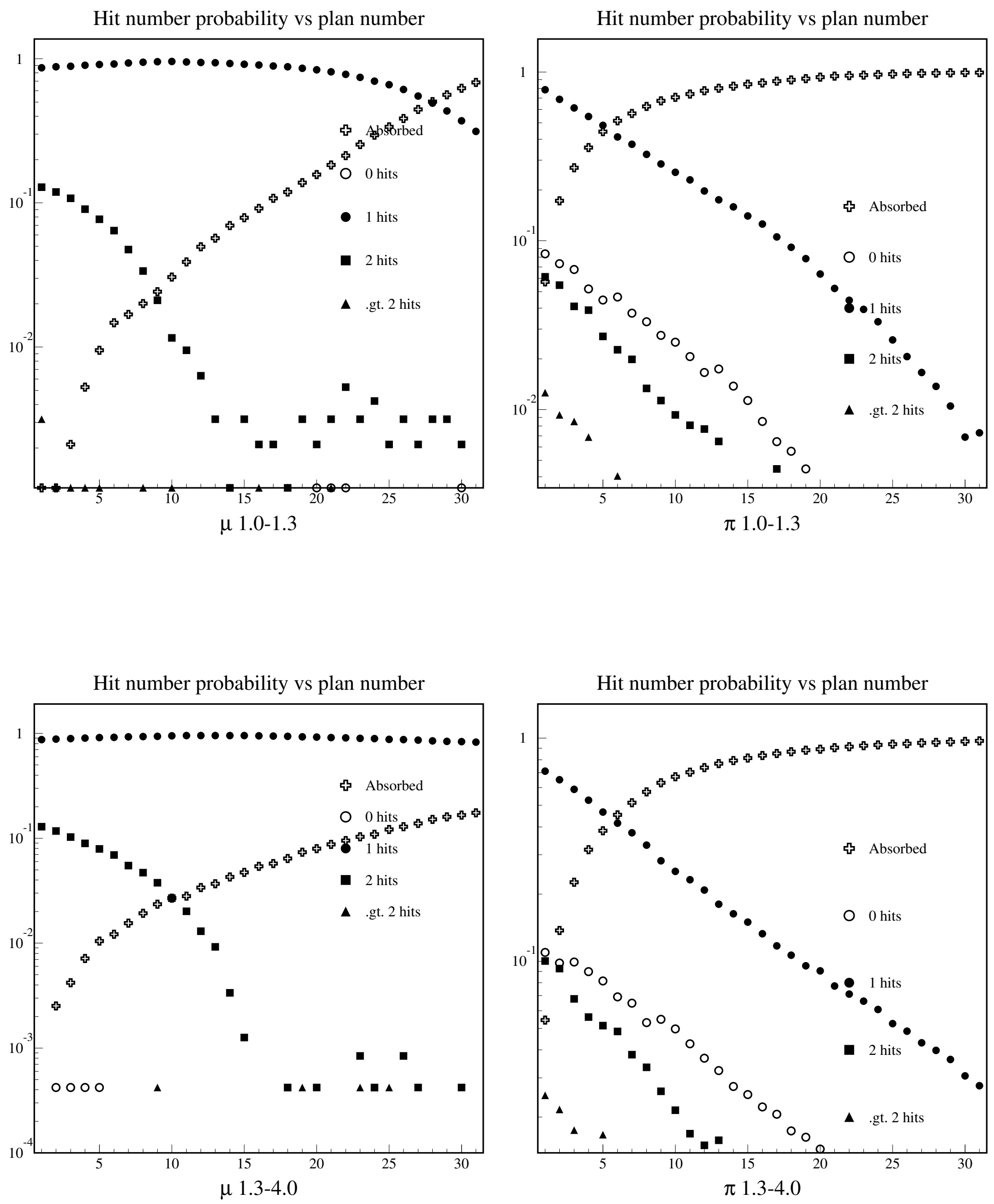

Figure 9: Probability distributions for the number of hits in each plane.

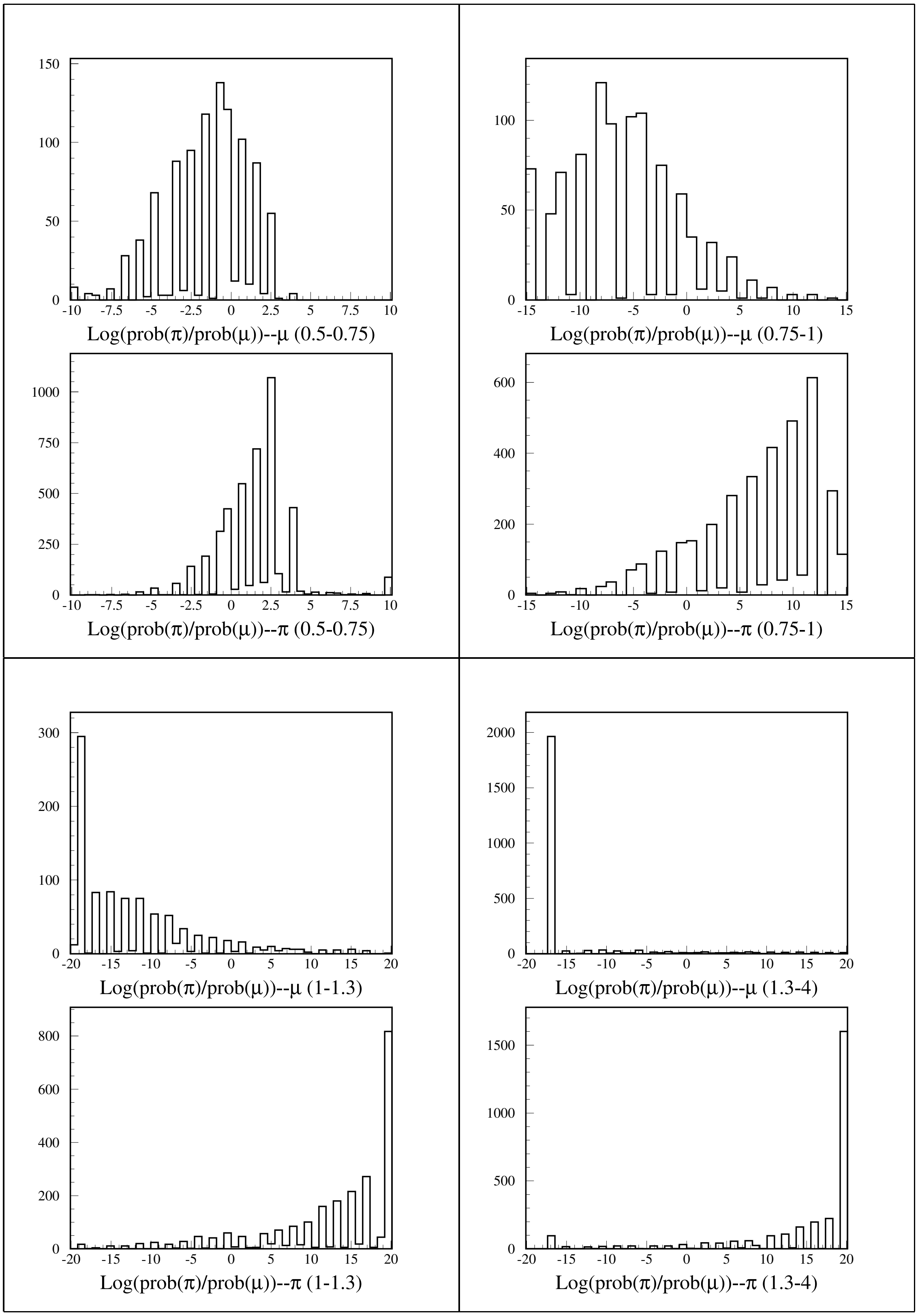

Figure 10: Likelihood function in the different momentum bins.

3.4 Tracking in the iron

Other means of discriminating μ's from π's can be obtained on the basis of tracking through out the iron. One can predict the behavior of on "ideal" track and then study the differences of pions and muons tracks with respect to the ideal case. The "ideal" approximation of a track giving hits in the barrel is different from one whose hits are in the endcaps (figure 11).

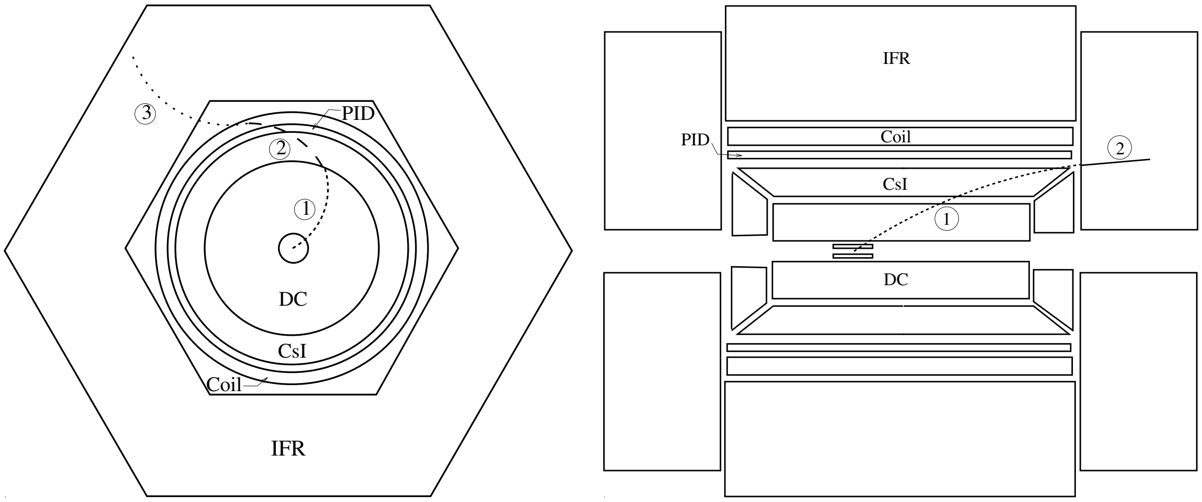

Figure 11: "Ideal" track approximation in barrel and endcaps

The former consist of three parts:

1. A piece of helix in the 1.5 T magnetic field with the `GEANT` momentum from the interaction point to the inner CsI radius.
2. An other piece of helix to the Coil radius with momentum corrected for the energy loss in the electromagnetic calorimeter (muon mass is given to the particle).
3. A succession of pieces of helix in the iron magnetic field, taking into account the energy loss in each iron plate.

The latter track (the endcaps one) can be approximated in a simpler (but poorer) way, since the magnetic field in the endcaps is more difficult to handle:

1. An helix (seen as a sinusoid in the side projection), from the interaction point to the plane of the first hit.
2. A straight line extrapolation of the helix starting from its entry point in the iron.

The parametrization of the difference between the extrapolated and the real track is made using the "residuals" function $\mathcal{R}$:

$$\mathcal{R} = \frac{1}{N_{\rm hit}} \sqrt{< |\vec{r}^{\,i}_{hit} - \vec{r}^{\,i}_{ext}|^2 >_{i=1\ldots N_{\rm hit}}}.$$

$\vec{r}^{\,i}_{hit}$ and $\vec{r}^{\,i}_{ext}$ are, respectively, the position of each of the $N_{\rm hit}$ hits and its predicted position. A cut for π rejection is applied on $\mathcal{R}$ as a function of the momentum, as plotted in figure 12.

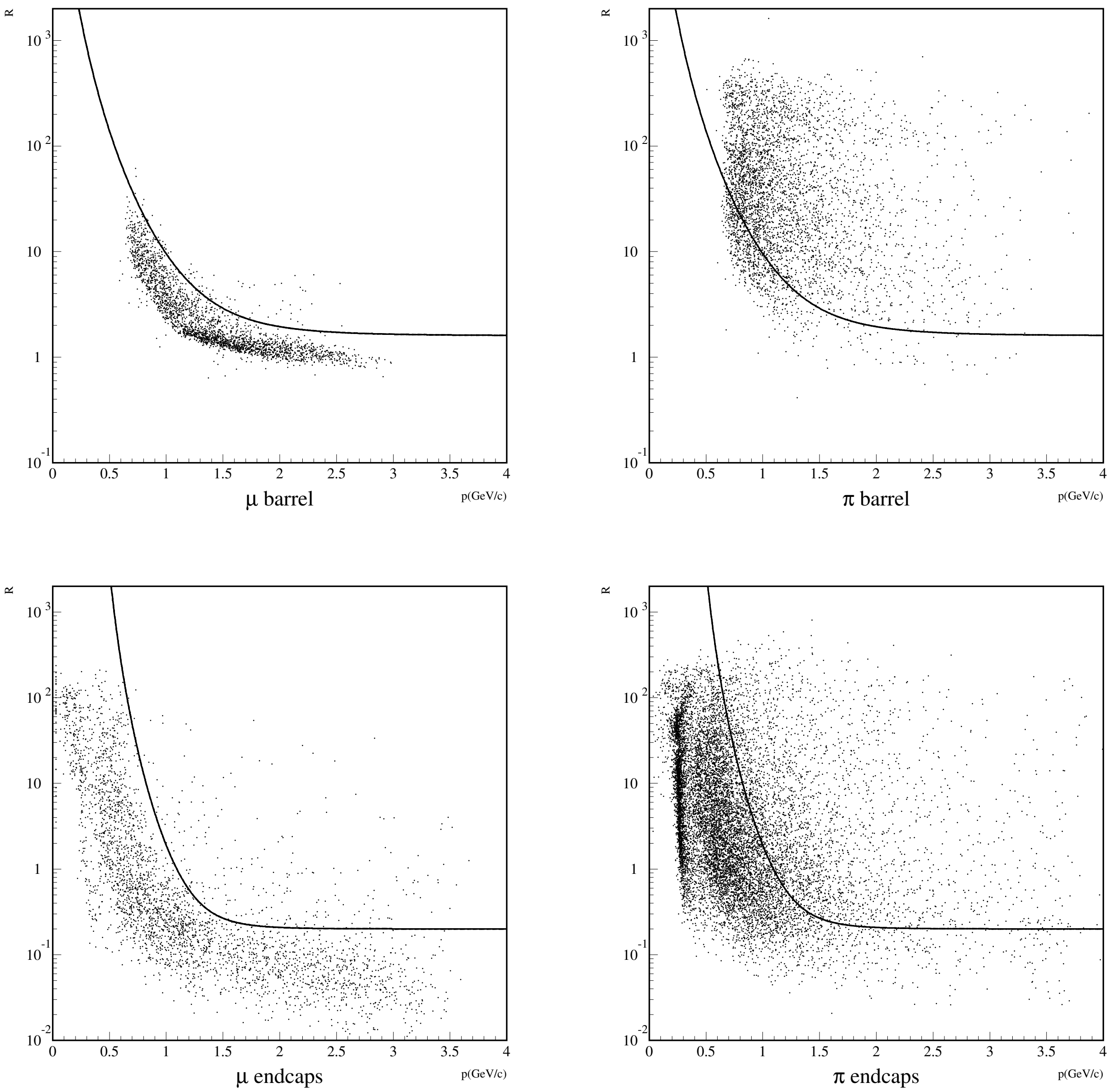

Figure 12: "Residuals" *vs* momentum in barrel and endcaps.

3.5 Inner detectors information

Energy loss in the drift chamber and in the CsI calorimeter have slightly different distributions for μ and π at low energy (figure 13) [5]. A cut on $(\mathrm{d}E/\mathrm{d}x)/p$ and on the energy loss in the CsI calorimeter, always normalized to the momentum, can reduce pion contamination paying a non negligible toll in muon efficiency. The effect of these cuts, however, is not relevant for the choice of the I.F.R. segmentation; one can resort to use them in analyses with very low π contamination requirements.

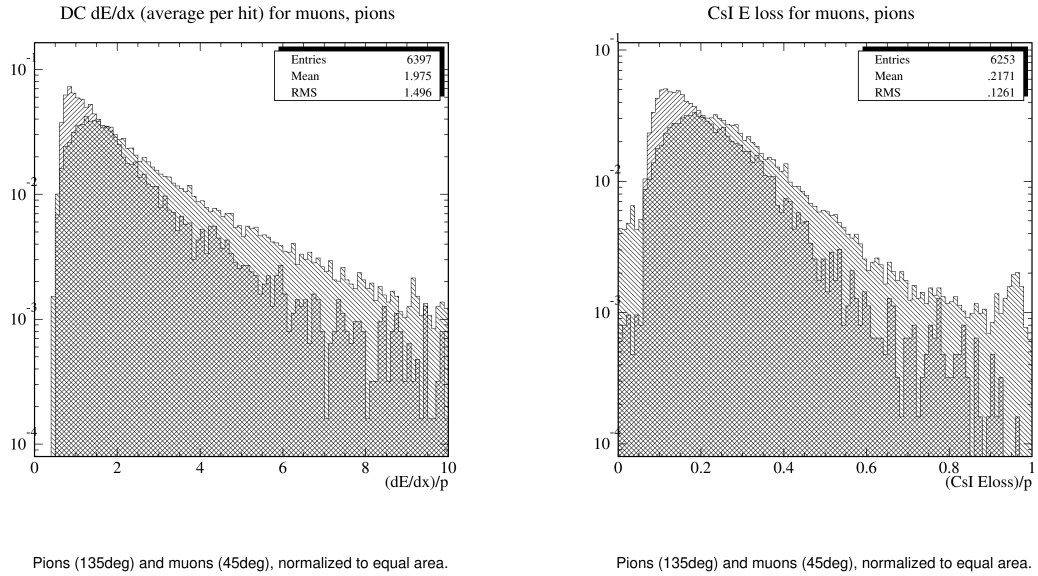

Figure 13: Left: $(\mathrm{d}E/\mathrm{d}x)/p$ (average per hit) for μ (hatched 45°) and π (hatched 135°). Right: energy loss in the CsI calorimeter over p. Distributions are normalized to 1.

3.6 Cuts

We can summarize the variables described above used for μ π discrimination:

- # of planes hit;
- material traversed (equivalent cm of Fe);
- # of planes spanned *minus* # of planes hit;
- # of consecutive missed planes along the track;
- $\log_{10}$ - likelihood ratio based on # of hits plane by plane;
- tracking "residuals".

On each variable a cut, that may depend on p, is applied (for material traversed the cuts depend also on θ). The cuts have been tuned in a different way for each of the segmentation configuration used.

4 Results with uniform segmentation

We optimized the selection criteria using the previously described variables for the 20×2 cm Fe planes in order to have the best signal to background ratio. We obtained a residual efficiency for pions of the order of 2% in the momentum range above 500 MeV/c (figure 14).

We tuned the selection for the other configurations keeping the same π efficiency, within errors, except for very low number of Fe planes (≤ 6) where the efficiencies both for μ and for π drop down just applying the minimum requirement of at least 3 planes hit for a μ identification.

The configurations with uniform segmentation studied are the followings:

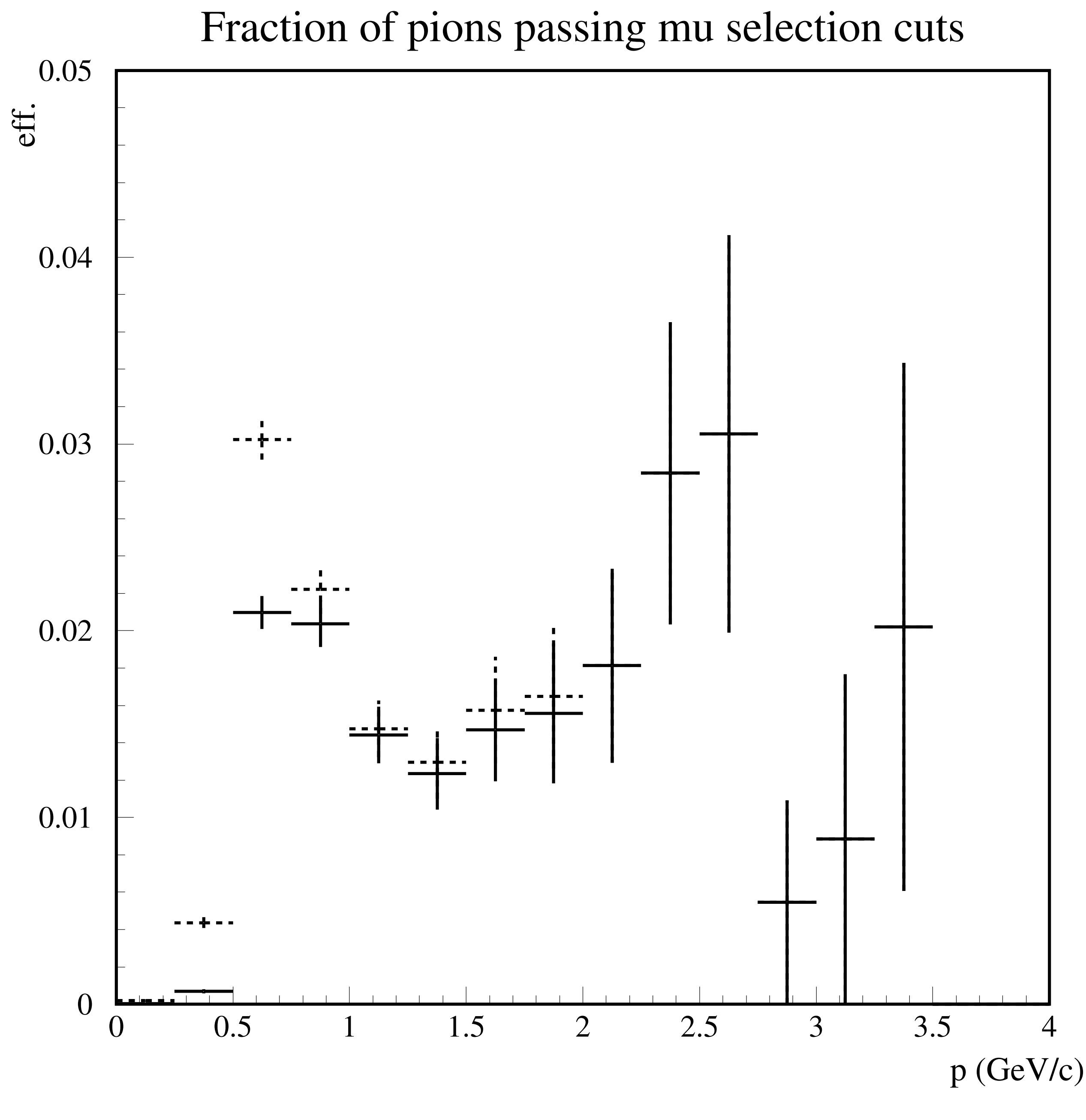

Figure 14: Pion efficiency as a function of momentum obtained for the 20×2 cm Fe planes configuration: solid: inner detectors cuts applied; dashed: no inner detectors cuts applied.

Fe planes	# of detector layers
30×2 cm	31
20×3 cm	21
15×4 cm	16
12×5 cm	13
10×6 cm	11
6×10 cm	7
5×12 cm	6
4×15 cm	5
3×20 cm	4

The efficiency for μ as function of momentum and number of detector layers is shown in figures 15 and 16. The efficiency curves as function of the momentum have been fit with the following function:

$$\varepsilon(p) = \frac{2A}{B + \exp(C/p)} \tag{1}$$

with A, B and C as free parameters.

Fe planes	A	B	C
30×2 cm	2838	5810	2.030
20×3 cm	4167	8565	5.263
15×4 cm	8956	18990	5.647
12×5 cm	36250	77980	6.682
10×6 cm	65920	143300	7.346
6×10 cm	16990	37450	7.658
5×12 cm	20040	45560	8.445
4×15 cm	971.9	2155	7.153
3×20 cm	14970	35400	11.070

Table 1: Fit values of A, B, and C; plateau efficiency ($p = \infty$) can be computed as $2A/B$.

Applying the inner detectors cuts causes a decrease of efficiency for for both π and μ with a modest signal to background improvement at low p. The comparison of figures 15 and 16 shows that inner detector cuts shift the efficiency curves of ~ 50 MeV/c towards higher p.

From the efficiency curves of figure 15 the effects of a thin segmentation are visible: for each fixed momentum value the efficiency drops down very rapidly decreasing the number of planes. The coarsest segmentation *"à la CLEO"* with four detector layers has about 30% efficiency at $p = 1$ GeV/c against 95% efficiency of the 21 layers configuration. For $p = 500 \div 600$ MeV/c the curves have an evident knee at 16 detector planes; the L.O.I. design with 25 detector planes sits well on the plateau. Reducing the number of planes clearly degrades the efficiency at low momenta and, to a lesser extent, at high momenta. It is also evident that increasing the segmentation up to 31 detector layers does not improve in a significant way muon efficiency.

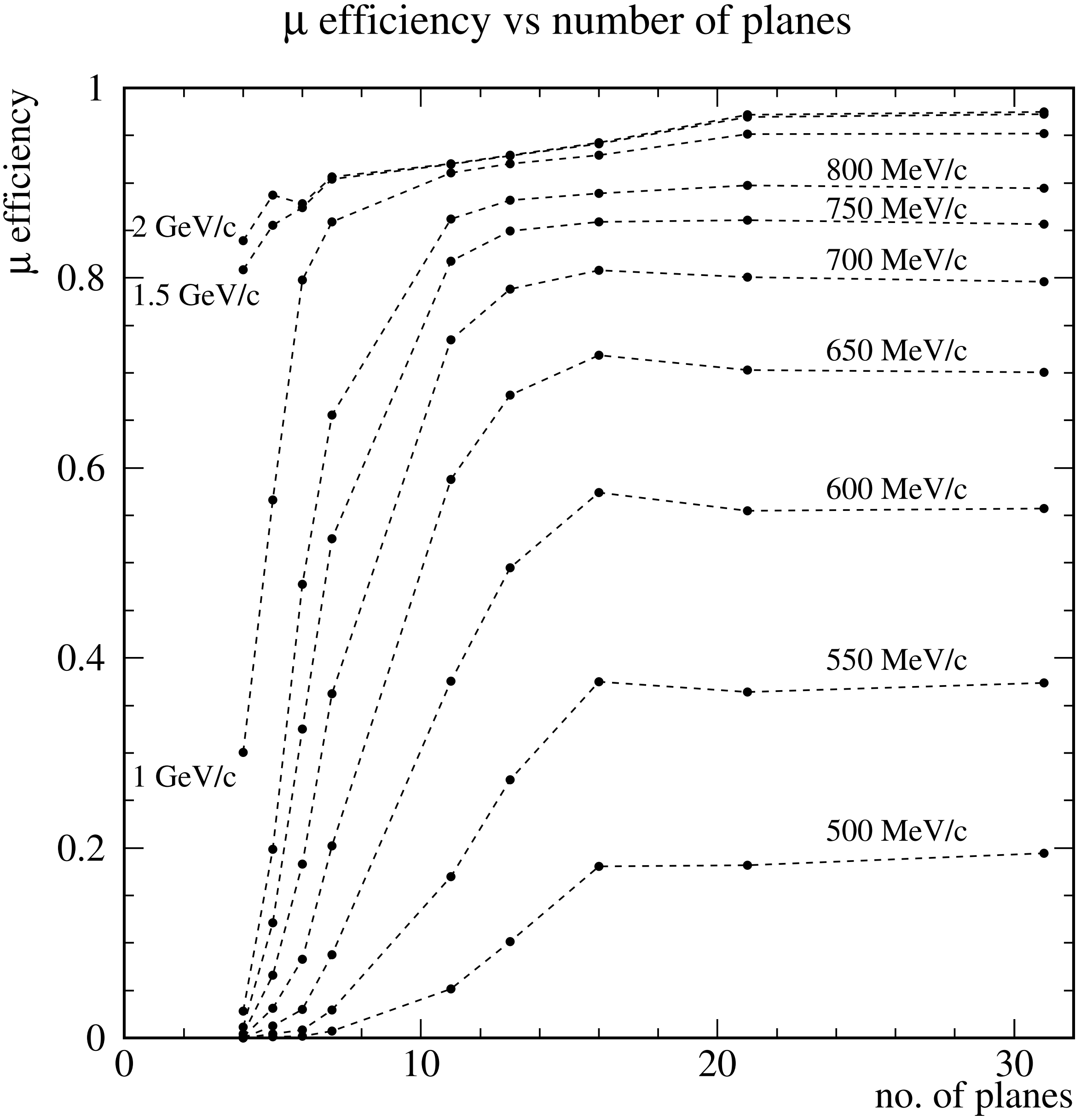

Figure 15: Muon efficiency as a function of the number of detector planes for fixed momentum value. Inner detector cuts are not applied.

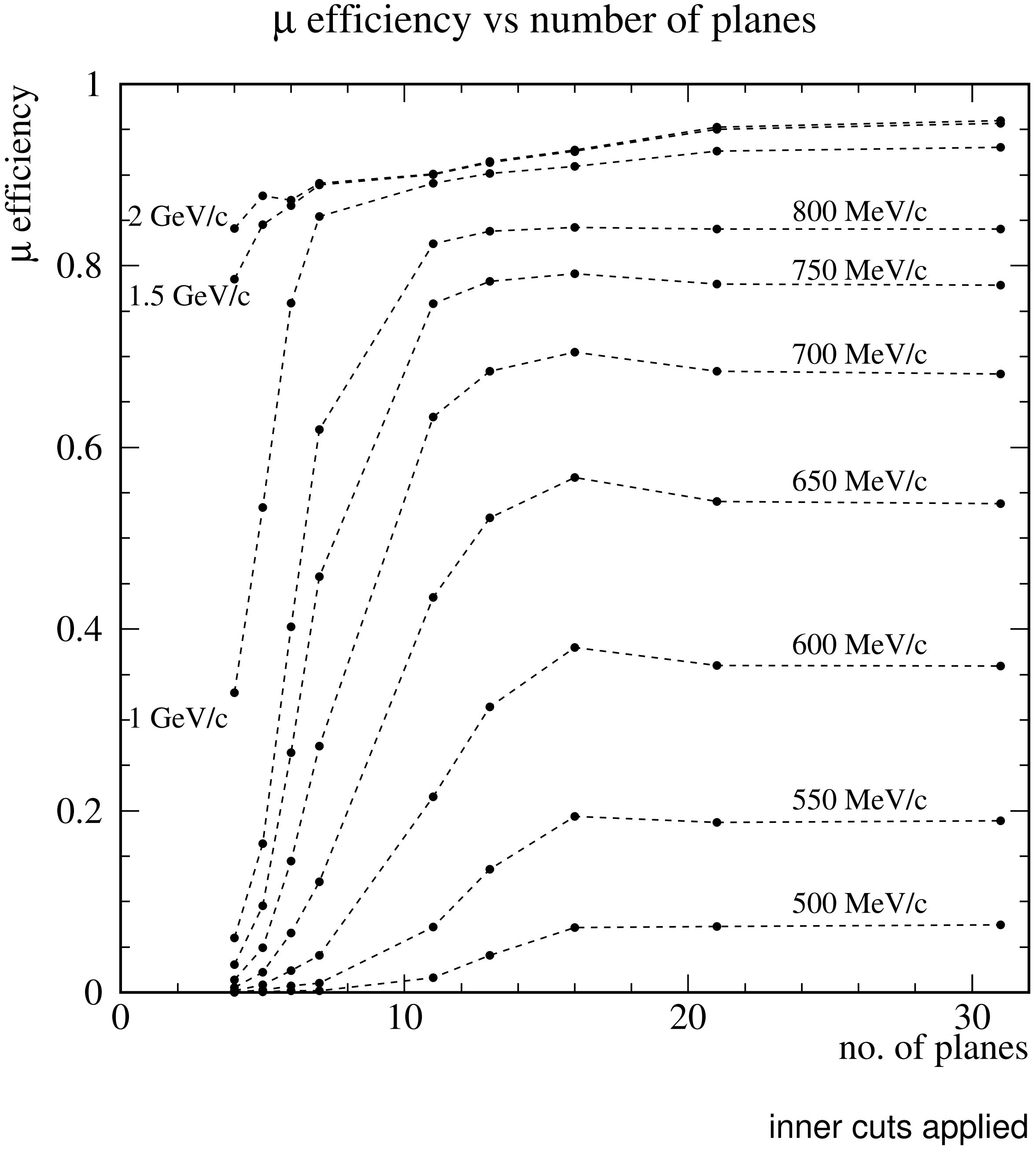

Figure 16: Muon efficiency as a function of the number of detector planes for fixed momentum value. Inner detector cuts are applied.

5 Graded segmentation

High segmentation is preferable especially for the identification of muons of low momentum. Since muons below ~ 1.3 GeV/c do not traverse all the iron, configurations with a thiner segmentation in the first planes, and a thicker one in the last planes can have as good performances as uniformly thin segmentation for low momenta giving a modest loss for high momenta. Moreover, pions stop mainly in the first part of I.F.R. and a thinner segmentation of the first layers improves π rejection.

We tried the following graded configurations with 15 and 20 Fe planes:

Fe planes	# of detector layers
10×2 cm + 5×8 cm	16
15×2 cm + 5×6 cm	21
10×2 cm + 5×3 cm + 5×5 cm	21
11×2cm + 6×3cm + 4×5cm	22

Muon efficiencies are shown in figures 17, 18 and 19; pion contamination has been kept at the value quoted in the previous section. In figure 17 one can see that the graded segmentation gives a global improvement in the efficiency. Figure 18 shows the results for 21 planes configurations.

Studies on K_L^0 detection efficiency show that graded segmentation configurations perform better than the uniform ones [8].

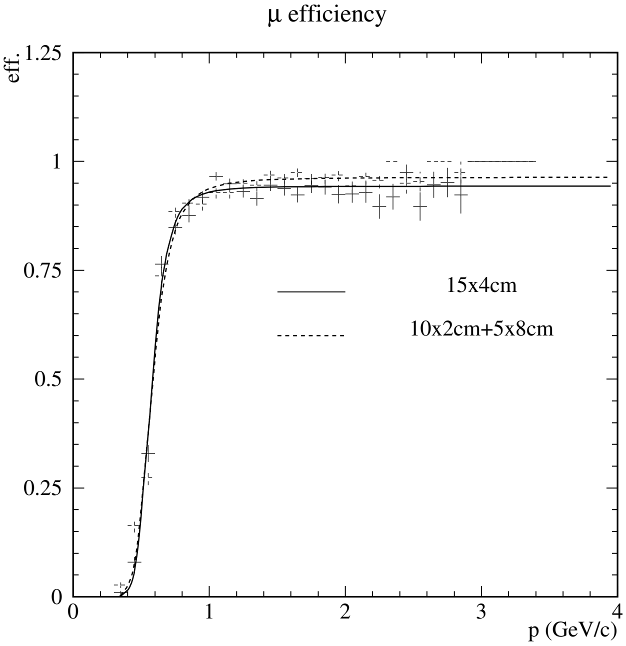

Figure 17: Muon efficiency as a function of momentum obtained for uniform and graded segmentations, with 15 Fe planes.

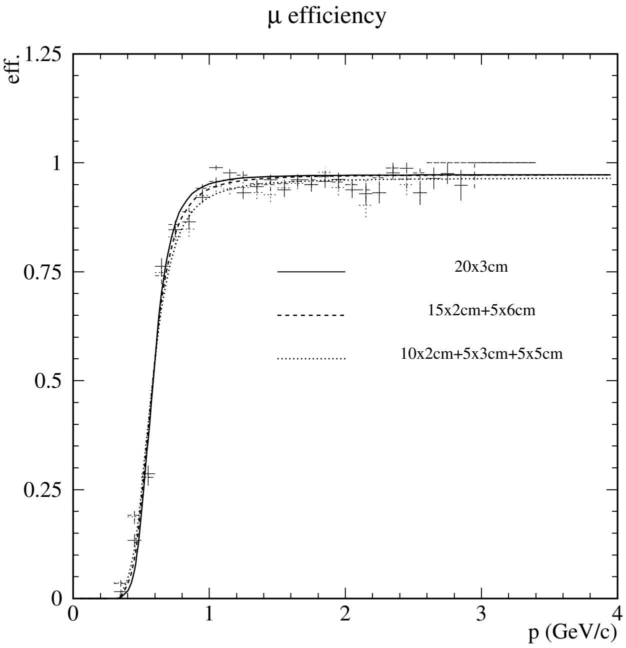

Figure 18: Muon efficiency as a function of momentum obtained for uniform and graded segmentations, with 20 Fe planes.

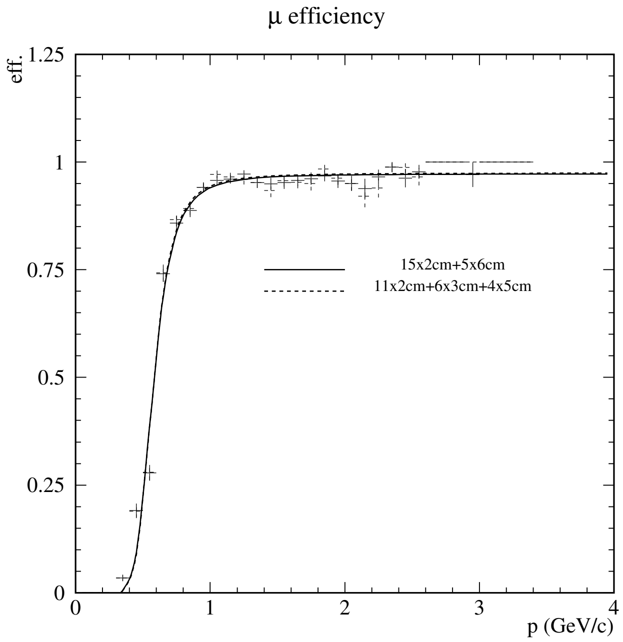

Figure 19: Muon efficiency as a function of momentum for the 11×2cm$+6 \times 3$cm$+4 \times 5$cm compared to 15×2cm$+5 \times 6$cm. The efficiency curves are almost identical.

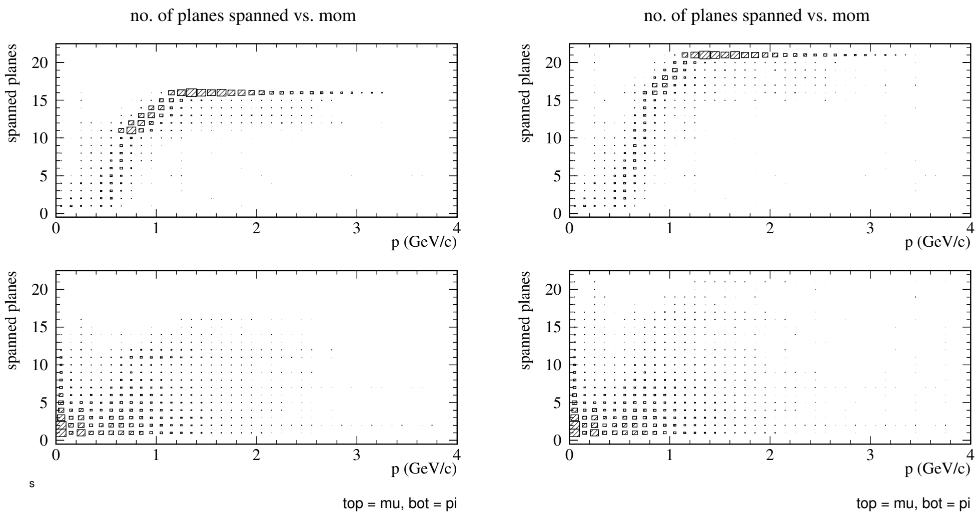

Figure 20: Planes spanned *vs* p in the 10×2 cm + 5×8 cm (left) and 15×2 cm + 5×6 cm (right) configurations.

6 Effect of detector inefficiency

Several variables used in our selection are subject to modification if the effect of single layer inefficiency is taken into account.

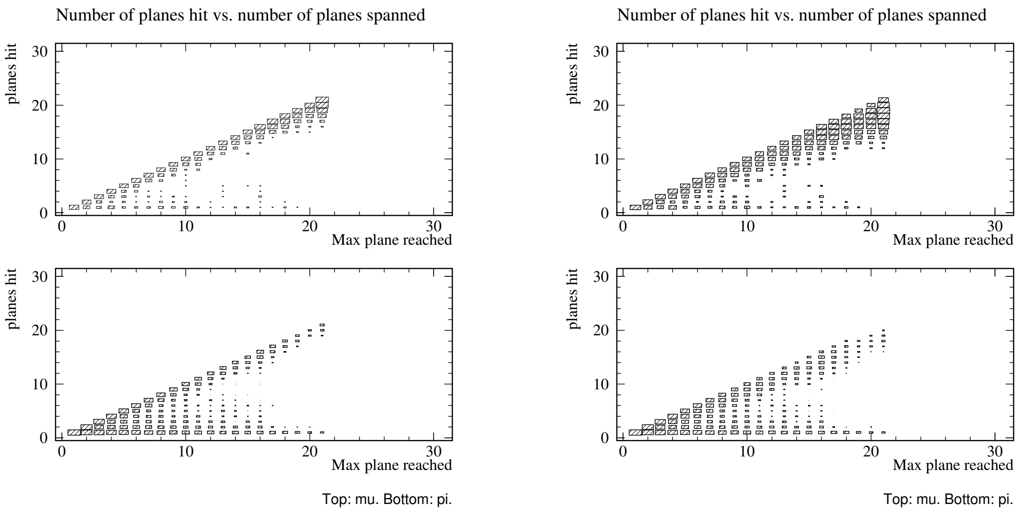

Figure 21: Span *vs* hit planes plot[1] obtained with 96% (left) and 87% efficiency (right).

[1]The size of the squares is proportional to the log of the number of entries.

For instance, figure 21 shows how the correlation of figure 5 is modified by detector inefficiency; the configuration 15×1 cm + 5×6cm is used. We used two values for $\varepsilon_{\mathrm{det.}}$: 96% and 87% which are close, respectively, to the efficiencies quoted for a single-gap RPC (including spacers and frames) and Plastic Streamers Tubes.

In order to recover the loss of rejection power due to layer efficiency, we re-tuned all the cuts to have the same π efficiency as for the previous cases. We obtain μ detection efficiencies shown in figures 22 and 23.

The effect of the 87% efficiency is a non negligible efficiency reduction over all the momentum range, especially at low p where cascade muons are more abundant.

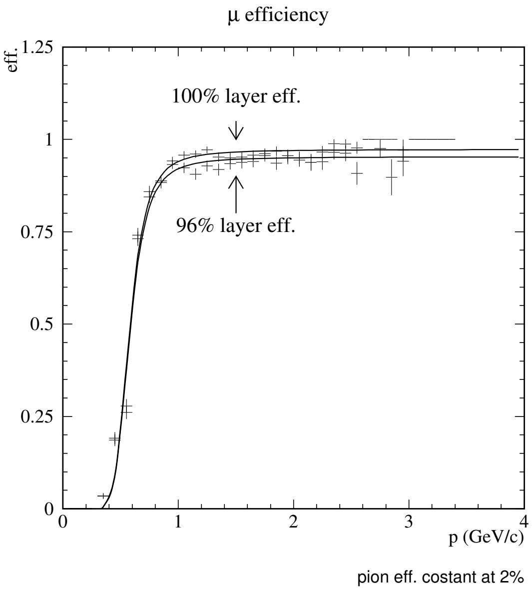

Figure 22: Muon efficiency as a function of momentum obtained with 96% efficiency.

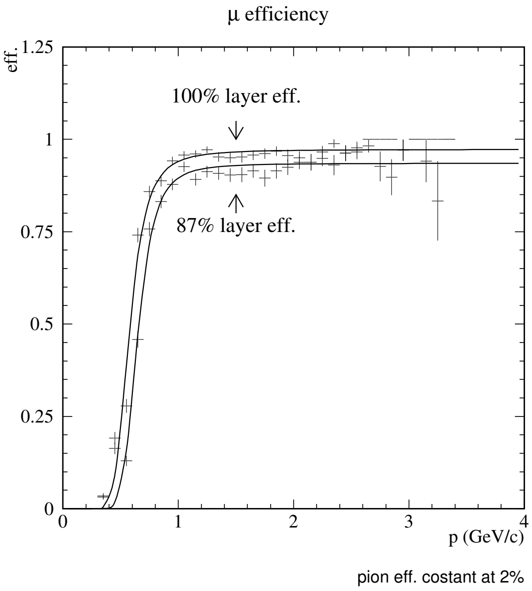

Figure 23: Muon efficiency as a function of momentum obtained with 87% efficiency.

7 Conclusions and outlook

We studied the effect of iron segmentation of the Instrumented Flux Return of BaBar detector on μ / π discrimination. We found optimal configurations around 20 Fe planes, and 21 detector layers. An efficient μ identification down to $p \sim 500$ MeV/c is obtained with a residual π efficiency of about 2%. We expect no dramatic decrease of efficiency if mono-gap RPC are to be used (96% layer efficiency) while the usage of lower coverage devices ($\varepsilon_{\mathrm{det.}}$=87%, as Plastic Streamer Tubes) would give a sensible loss of efficiency both at low and high momenta.

A preliminary study done separately on the barrel and the two endcaps shows a non uniform pion contamination in the three subsystems. Residual pi efficiency is approximately constant at 1.5% over the entire momentum range in the barrel, while it seems to be higher ($\approx$ 3.5%) in the forward endcap. The possibility of adding more iron to the forward (backward) end caps must be thoroughly evaluated.

From the same study it can also be seen that muon detection efficiency at low momenta is lower in the barrel than in the endcaps; this is probably due to particle absorption in the superconducting coil. An improvement in μ efficiency at low momenta can be obtained inserting detector layer(s) in front of the cryostat [9].

8 Acknowledgements

We are grateful to Ida Peruzzi, Marcello Piccolo and Crisostomo Sciacca for useful suggestions and discussions; we also thank Torre Wenaus and Douglas Wright for their patient help in the installation and usage of `bbsim`. A special thank to Corrado Gatto who helped us developing the Fe-tracking code.

References

[1] M.G. Pia; BABAR note # 192 in preparation.

[2] D. Wright; talk at SLAC meeting sep. 94, posted on World-Wide Web at the URL: `http://babar1.llnl.gov/wright/talks.html#t1`

[3] T. Wenaus; The `bbsim` Hypertext Manual, posted on World-Wide Web at the URL:
`http://www.slac.stanford.edu/BFROOT/src/bbsim/bbsim/doc/bbsim.html`

[4] D. Wright; `beget`: The B-Factory Event Generator - Version 21; BABAR note # 149 and `beget` posted on World-Wide Web at the URL:
`http://babar1.llnl.gov/wright/doc/beget.html`

[5] Conceptually similar analyses have been presented by T. Wenaus; posted on World-Wide Web at the URL:
`http://babar1.llnl.gov/wenaus/hz/muid.html`

[6] V. Innocente, M. Maire and E. Nagy; GEANE - Average Tracking and Error Propagation Package; L3 Report #572.

[7] A. Calcaterra; BABAR note #144.

[8] R. De Sangro, A. Zallo; Pisa meeting oct. 94.

[9] T. Wenaus; Pisa meeting oct. 94.